https://doi.org/10.5194/angeo-2019-152
Preprint. Discussion started: 7 November 2019

Annales Geophysicae Discussions
Open Access
EGU

Earth's radiation belts ions: Patterns of the spatial-energy structure and its solar-cyclic variations

Alexander S. Kovtyukh
Skobeltsyn Institute of Nuclear Physics, Moscow State University, Moscow, 119234, Russia;
kovtyukhas@mail.ru

Abstract Spatial-energy distributions of the stationary fluxes of protons, helium ions and ions of carbon-nitrogen-oxygen (CNO) group, with energy from $E \sim 100$ keV to 200 MeV, in the Earth's radiation belts (ERB), at $L \sim 1$–8, are considered here by the data of the satellites for 1961–2017. It is find that the results of these measurements line up in the space $\{E, L\}$ by some regular patterns. Solar-cyclic (11-year) variations in the distributions of protons, helium ions and CNO group ions fluxes in the ERB are studied. In the inner regions of the ERB the ions fluxes decrease with increasing solar activity. It is find, the solar-cyclic variations of fluxes for ions with $Z \geq 2$ are much greater than for protons and increase with increasing an atomic number Z of the ions. The possible physical mechanisms leading to formation of this spatial-energy structure and to the solar-cyclic variations of the ERB ion fluxes are discussed.

Keywords. Magnetospheric physics (energetic particles, trapped). Radiation belts.

1 Introduction

The Earth's radiation belts (ERB) consist of charged particles with energy from E ~ 100 keV to several hundreds of megaelectronvolt (MeV). These particles are trapped by the geomagnetic field at altitudes from ~ 200 kilometers to ~ 50–70 thousands kilometers. The ERB is consisted mainly from electrons and protons. In the ERB there are also ions of helium, oxygen, and other elements with the atomic number $Z \geq 2$, where Z is the charge of the atomic nucleus with respect to the charge of the proton. During geomagnetic disturbances a fluxes of ions and its distributions are varied. These fluxes depend also on the phase of the solar cycle, conditions in the interplanetary space, and other factors.

Particles with different energy E and pitch angles α (α is the angle between a local vector of the magnetic field and vector of a particle velocity), which injected into some point of the geomagnetic trap, are drifted with conserving the adiabatic invariants (μ, K, Φ) and populate a narrow layer surrounding the Earth (Alfvén and Fälthammar, 1963; Northrop, 1963). This layer call the drift shell. Therefore, experimental data on the ERB do most simply represented in coordinates $\{L, B\}$, where L is parameter of a drift shell and B is a local induction of the magnetic field (McIlwain, 1961). For the dipole magnetic field L is a distance, in the equatorial plane, from the given magnetic field line to the center of the dipole (in the Earth's radii R_E).

The stationary fluxes J of the ERB particles with given energy and pitch angle α are decreased usually when the point of observation is shifted from the equatorial plane to a higher latitudes along certain magnetic field line (if we exclude the peripheral regions of the geomagnetic trap, where the drift shells of the captured particles are split and branched). This dependence of the particle fluxes is described by the functions $J(B/B_0)$, were B and B_0 are values of the magnetic field at the point of observation and in the equatorial plane on the same magnetic field line.

Outer and inner regions of the ERB maintained in the dynamic equilibrium with the environment by the different mechanisms (see review Kovtyukh, 2018).

The outer belt ($L > 3.5$) of ions is formed mainly by the mechanisms of the radial diffusion of these ions to the Earth under the action of fluctuations of an electric and magnetic fields resonating with a drift periods of these ions. This transport accompanied by the betatron acceleration of ions and by the ionization losses of the ions in result of their interactions with the plasmasphere and with residual atmosphere.

The inner belt ($L < 2.5$) of protons with $E > 10$ MeV is formed mainly as a result of decay of neutrons knocked from the nuclei of the atmospheric atoms by the Galactic Cosmic Rays (GCR). For protons with $E < 10$ MeV this mechanism (CRAND) is supplemented by the radial diffusion of particles from the outer to the inner belt. The inner belt of ions with $Z > 4$ was formed mainly from the ions of the Anomalous component of Cosmic Rays (ACR).

In the intermediate region ($2.5 < L < 3.5$) is operated also the mechanism of a capture of the ions from the Solar Cosmic Rays (SCR) during strong magnetic storms (see, e.g., Selesnick et al., 2014).

Thus, the main mechanisms of formation of the ERB, sources and losses of the ions are known. However, for the comprehensive verification of the physical models and to identification of the mathematical models parameters it is necessary sufficiently complete and reliable empirical models of the ERB for each of ion components. It is necessary also for ensuring the safety of space flights.

These models can be created only on a basis of the experimental data are obtained over many years and decades. Such models (see, e.g., Ginet et al., 2013) were created for protons (AP8/AP9). These models are widely used in the space research. However, measurements of fluxes of the ions with $Z \geq 2$ are represented a difficult technical problem due to a small fluxes of these ions and high background fluxes of protons and electrons. The empirical and semi-empirical models of the ERB developed for ions with $Z \geq 2$ are applicable only to very limited regions of the space $\{E, L\}$.

https://doi.org/10.5194/angeo-2019-152
Preprint. Discussion started: 7 November 2019

Annales Geophysicae Discussions

There are problems connected with limited and incomplete information on the fluxes of ions with $Z \geq 2$ in the ERB, especially in the energy range from tens to hundreds of megaelectronvolt. One of the main problem of this work is to consider the possibility to create sufficiently complete and reliable empirical models of the ERB for these ions based on currently available world experimental data.

In the following sections are considered the spatial-energy structure of the ERB in the spaces $\{E, L\}$ for protons, helium ions and ions of the CNO group on the experimental data (Sect. 2), possible physical mechanisms of formation of these structures and its solar-cyclic variations are discussed (Sect. 3) and the main conclusions of this work are given (Sect. 4).

2 Spatial-energy distributions of the ion fluxes near the equatorial plane

There can be trapped on the drift shells only ions with energy less than some maximum values determining by the Alfvén's criterion: $\rho_i(L, E, M_i, Q_i) << R_c(L)$, where ρ_i is the gyroradii of ions, and R_c is the radius of curvature of the magnetic field near the equatorial plane (M_i and Q_i are mass and charge of ions with respect to the corresponding values for protons). According to this criterion and the theory of stochastic motion of particles, the geomagnetic trap can capture and durably hold only ions with E (MeV) < $2000\times(Q_i^2/M_i)\ L^{-4}$ (Ilyin et al., 1984). The green line is present this boundary on Figs. 1–6.

When comparing the data of various experiments in the ERB, the question arises about the compatibility of these results with each other and the reasons for their discrepancies. More or less significant discrepancies in the results of the satellites can be connected with the differences in the trajectories of the satellites; in the construction of the instruments and their angular characteristics; in the energy ranges and sets of the energy channels. For the stationary ERB, these discrepancies can also be associated with differences in the general state of the Solar, heliosphere and magnetosphere of the Earth at the different measurements periods. These factors influence on the fluxes of ions with $Z \geq 2$ in the ERB more significantly than on the proton fluxes (see, e.g., Kovtyukh, 2018).

This section used experimental data of various satellites, which were obtained for quiet periods (Kp < 2) and near the equatorial plane of the ERB for ions with equatorial pitch angles $\alpha_0 \approx 90^{\circ}$. The preference was given to the averaged results of these satellites for quiet periods. All values of differential fluxes reduced to one dimension. In the regions of E and L shells where these data were obtained the ion fluxes do not distorted by the background of other particles.

In many important experiments, the instruments did not allow separate fluxes of ions by charge of ions. For ions of the CNO group the separation by mass also are not performing usually. For heavier ions, for example for Fe ions, we have very smaller such data. Therefore, this work presents only helium ions (without separating them by charge) and ions of CNO group (without separating them by mass and charge).

To solve the problems considered here, it is important to choose the form of representation (space of variables), in which the results of different experiments can be conformed to each other naturally. For such representation of the distributions of the ion fluxes have been chosen the space $\{E. L\}$. Such representation is possible to organize of a fragmentary experimental data obtained in different ranges of E and L most effectively.

Figures 1–6 presented here the spatial-energy distributions of the fluxes of protons, helium ions, and ions of the CNO group near the equatorial plane. These figures are paired: odd figures refer to periods near the minima, and even figures refer to periods near the solar activity maxima. The values E and L in these figures are presented in logarithmic scales. Experimental points on these figures connected by lines of the equal intensity of ion fluxes (iso-lines); the decimal logarithms of the fluxes J are shown near each iso-lines. The ion fluxes J have a dimension (cm^2 s ster MeV/n)$^{-1}$ and are corresponded to the energies E (MeV/n) and an equatorial pitch angle of α_0 is ~ 90°.

https://doi.org/10.5194/angeo-2019-152
Preprint. Discussion started: 7 November 2019

Such representations of the experimental data are not only visual, but also are very convenient and rather universal. Obviously, Figs. 1–6 actually show both radial profiles of the fluxes of ions for a given energy (if one see along the abscissa axis) and ion energy spectra for a given L shell (if one see along the ordinate axis).

In this place, it is need to say a few words about the method of constructing these figures. The points in Figs. 1–6 are obtained from the dependences $J(L)$ for a given ions with a certain energy (the average energy for each channel) and with an equatorial pitch angle close to 90^{o}. Unlike a distributions of electrons, as well as ion distributions connected with magnetic disturbances, the dependences $J(L)$ for the ERB ions with $\alpha_0 \sim 90^{o}$ usually have only one maximum in a quiet time. As a result, for each experiment 1 or 2 points were obtained (on the outer and inner edges of this profile) with certain values of E and L for a given level of stationary ion fluxes. Sometimes, especially for low levels of fluxes, only one point was obtained: in these cases, the radial profile of the ion fluxes was cutoff at small L by a significant background of other particles. In these cases, no interpolations and extrapolations of the radial profiles of ion fluxes does performing here.

Each iso-line shown in these figures was built separately, for the corresponding set of experimental points (icons); after that this iso-line was transferred (along with the icons) to the corresponding figure. Thus, in the region abundantly populated by such icons (for protons with $E >$ 1 MeV at $L > 2$) they are mixing in Figs. 1–2. In the cases of a large distances between neighbor points, the corresponding segments of the iso-lines are shown in dotted arcs in these figures.

The radial profiles of the differential fluxes $J(L)$ shown on uniform presentation for particles of different energies are intersect with each other in those regions where the energy spectra of these fluxes are have a local maximum or minimum. In contrast, the flux iso-lines cannot intersect each other: this would mean that at the same point in the space $\{E, L\}$ the proton fluxes differ very significantly (by an order of magnitude for the flux step selected here). Such uncertainty does not have a physical sense and means a complete discrepancy and contradiction to each other of two close series of data obtained in different experiments. In this case, a special analysis is needed to identify all the errors and differences in the conditions for different measurements, in order to reconcile them with each other.

The largest errors of our method are connected with drawing iso-lines of fluxes along heterogeneous sets of experimental points (the errors of these points themselves do not exceed of the size of the icons on Figs. 1–6). This uncertainty of our work is open for constructive criticism, and these figures themselves are open for possible corrections and additions.

The synthesis of the experimental data on the fluxes of ERB ions in other representations (in other spaces of variables) leads to more significant methodological errors and uncertainties. For example, one can present ion fluxes obtained in various experiments for different energy channels depending on L (radial profiles of fluxes). However, the sets of these channels are different in different experiments. To compare the radial profiles of ion fluxes for different experiments, it is necessary to bring these fluxes to the same set of energy values. This can made by energy spectra, but due to discreteness of these spectra, the procedures of their approximation, interpolation, and extrapolation are inevitable. But this work can be done in different ways. With that, methodical errors and uncertainties in the final picture acquire a hidden form. They can be tracked only if consistently, step by step, repeating all these procedures for the experimental data.

2.1 Spatial-energy structure of the proton fluxes

There is a great quantity of the experimental data on the ERB protons. The most important of them are presented in the space $\{E. L\}$ on Figs. 1 and 2. These figures are needed here for comparison with similar distributions of ions with $Z \geq 2$ on the Figs. 3–6.

Figure 1 represent a results of the satellites Relay-1 (Freden et al., 1965); Ohzora or EXIS C: Exospheric Satellite C, Akebono or EXOS-D: Exospheric Satellite D and ETS-VI: Engineering Test

https://doi.org/10.5194/angeo-2019-152
Preprint. Discussion started: 7 November 2019

Annales Geophysicae Discussions

Satellite (Goka et al., 1999). These results were obtained near minima between 19th and 20th (1963), 21th and 22th (1984–1985), and 22th and 23th (1994–1996) of the solar activity cycles.

Figure 2 represent a results of the satellites 1968-81A (Stevens et al., 1970), Injun-5 or Explorer-40 (Krimigis, 1970; Venkatesan and Krimigis, 1971; Pizzella and Randall, 1971), 1969-025C or OV1-19: Orbiting Vehicle 1-19 (Croley et al., 1976), Azur or GRS A: German Research Satellite A (Hovestadt et al., 1972; Westphalen and Spjeldvik, 1982), Molniya-1 (Panasyuk and Sosnovets, 1973), GEOS-2: Geodetic Earth Orbiting Satellite 2 (Wilken et al., 1986), CRRES: The Combined Release and Radiation Effects Satellite (Albert et al., 1998; Vacaresse et al., 1999), GEO-3: Geostationary Orbit 3 (Selesnick et al., 2010) and Van Allen Probes (Selesnick et al., 2014, 2018). These results were obtained near maxima of solar activity in 20th (1968–1971), 22th (1990–1991), 23th (2000), and 24th (2012–2017) solar cycles.

The data of the satellites Explorer-45 (Fritz and Spjeldvik, 1979, 1981) and ISEE-1: International Sun-Earth Explorer 1 or Explorer-56 (Williams, 1981; Williams and Frank, 1984) are given in Figs. 1 and 2 at $L > 2.5$ where solar-cyclic variations of the ERB proton fluxes are practically do not observed (see, e.g., Vacaresse et al., 1999).

Other experimental data on ERB protons could be added to these results, but they do not change the general picture shown in Figs. 1 and 2.

From a comparison of Figs. 1 and 2 one can see that at $L < 2.5$ (especially at $L < 1.4$) the proton fluxes in the minima of solar activity (Fig. 1) are higher than in the maxima of solar activity (Fig. 2). In addition, in the minima of solar activity the inner edge of the proton belt is less steep and achieve smaller L shells (for $E > 1$ MeV). The distribution functions of protons $f(\mu, K, L)$ in the phase space constructed from Figs. 1 and 2 confirm these conclusions.

In Figs. 1 and 2, the iso-lines of proton fluxes are almost parallel to each other on $L > 3$ at sufficiently high energies. Since these iso-lines are separated from each other by approximately equal intervals on a logarithmic scale of the energy, this region in the space $\{E. L\}$ corresponds to power-law spectra of the ERB protons. In these figures, this region is located between the green and red lines.

The red line is corresponded to the lower boundary (E_b) of the power-law tail of the proton spectra. For this line, $E_b \sim 36{\times}L^{-3}$ MeV. Some changes in the slope of these iso-lines at $L > 6$ can be connected with an essential distinction of the magnetic field in this region from the dipole configuration (the L shells were calculated for a dipole field).

For the dipole magnetic field region, the points on the red line correspond to particles with a specific value of the 1st adiabatic invariant of motion (μ_b). For Figs. 1 and 2, the average value μ_b is ~ 1.16 keV nT^{-1}. Segments of an iso-lines that are parallel to the red line also correspond to a certain values of the invariant μ. In this region of the space $\{E. L\}$ the ionization and other losses of the ERB protons during radial drift can be neglected, and the fluxes changes with changing of L are practically reduced to adiabatic transformations the fluxes in a magnetic field.

It is results from these figures that at $L = 3$–6 the value $\gamma = 4.8 \pm 0.5$. At $L > 6$ the distances between these iso-lines are increased with L, and the value γ is decreased from ~ 4.7–5.0 at $L = 6$ to ~ 4.1–4.5 at $L = 8$. This is due to the deviation of the magnetic field from the dipole configuration as well as to the increasing variability of this field with increasing L.

According to the data of satellites considered in (Kovtyukh, 2001), invariant parameters μ_b and γ were found only at $L > 3$. In this work is considered the wider range of L and E, and for protons with $E > 10$ MeV these parameters can be traced to $L \sim 2$. At $L = 2$, $\gamma = 4.4 \pm 0.6$ (Fig. 1) and $\gamma = 4.7 \pm 1.3$ (Fig. 2). This is due to that the energy range here is significantly extended toward higher energies (up to 200 MeV), but with increasing the energy of the ERB protons the ionization losses are decreased rapidly (see, e.g., Schulz and Lanzerotti, 1974; Kovtyukh, 2016a).

https://doi.org/10.5194/angeo-2019-152
Preprint. Discussion started: 7 November 2019

2.2 Spatial-energy structure of the helium ion fluxes

In Figs. 3 and 4 are presented helium ions fluxes averaged for quiet periods (Kp < 2).

Figure 3 represent the data of the satellites Molnija-2 (Panasyuk et al., 1977), Prognoz-5 (Lutsenko and Nikolaeva, 1978), ISEE-1: The International Sun-Earth Explorer 1 (Hovestadt et al., 1981); Akebono or EXOS-D: Exospheric Satellite D and ETS-VI: Engineering Test Satellite (Goka et al., 1999). These results were obtained near minima between 20th and 21th (1975–1977)), between 21th and 22th (1984–1985), and between 22th and 23th (1994–1996) of the solar activity cycles.

Figure 4 represent the data of the satellites OV1-19: Orbiting Vehicle 1-19 (Blake et al., 1973; Fennell and Blake, 1976), Explorer-45 (Fritz and Spjeldvik, 1978, 1979; Spjeldvik and Fritz, 1981), SCATHA: Spacecraft Charging At High Altitudes (Blake and Fennell, 1981; Chenette et al., 1984). These results were obtained near maxima of solar activity in 20th (1968–1971) and 21th (1979) solar cycles.

From a comparison of Figs. 1–2 with Figs. 3–4 one can see that at $L > 2$ for helium ions the solar-cyclic (11-year) variations are greater than for protons. For example, at $L \sim 2$–3 from maximum to minimum of solar activity fluxes of protons with $E > 1$ MeV practically do not changed, and the fluxes of helium ions with $E > 1$ MeV/n are increased by one order of magnitude.

Figures 3 and 4 have the same patterns are observed as for protons, but the distribution of helium ion fluxes is slightly shifted away from the Earth (with respect to protons). Unlike protons, there are significant “white spots” for helium ions in this picture.

The red line on these figures is corresponded to the lower boundary of the power-law tail of the helium ions spectra. For this line, $E_b/M_i \sim 43.4{\times}L^{-3}$ MeV/n (Fig. 3) and $E_b/M_i \sim 21.7{\times}L^{-3}$ MeV/n (Fig. 4). If one take into account that for helium ions with $E > 0.2$ MeV/n at $L < 6$ the average charge Q_i is +2 (see, e.g, Spjeldvik, 1979), then for the considered boundary we get: $\mu_b \sim 1.4{\times}Q_i$ keV/n×nT^{-1} at the maximum of solar activity and $\mu_b \sim 1.4{\times}M_i$ keV/n×nT^{-1} at the minimum of solar activity (for the dipole magnetic field region). The iso-lines of helium ion fluxes in Figs. 3 and 4, which pass above the red line at $L > 2.5$ are corresponded average value of $\gamma \sim 5.5$.

For helium ions, as for protons, the values of the parameters of the power-law tail of their spectra are approximately in the middle of the ranges of these parameters, which were obtained by other methods (Kovtyukh, 2001).

At the same time, one can see that the isolines of the fluxes of helium ions in the region above the red line (in the region of power-law spectra) have at a substantial slope to the red line. At $L > 3$ the fluxes of helium ions with given energy are increased with decreasing L more slowly than follows from adiabatic transformations of the fluxes. In accordance to well-known calculations (see, e.g., Schulz and Lanzerotti, 1974), this is means that the ionization losses of the ERB helium ions significantly exceed these losses for protons.

2.3 Spatial-energy structure of the CNO group ions fluxes

In Figs. 5 and 6 are presented CNO group ions fluxes averaged for quiet periods (Kp < 2).

Figure 5 represent the data of the satellites ATS-6: Applications Technology Satellite 6 (Spjeldvik and Fritz, 1978; Fritz and Spjeldvik, 1981) and ISEE-1: The International Sun-Earth Explorer 1 (Hovestadt et al., 1978). These results were obtained near the minimum between 20th and 21th of the solar activity cycles (1974–1975, 1977).

Figure 6 represent the data of the satellite Explorer-45 (Spjeldvik and Fritz, 1978; Fritz and Spjeldvik, 1981). These results were obtained near the maximum of solar activity in 20th solar cycle (1971–1972).

On Figs. 5–6 the spatial-energy patterns of the fluxes for the CNO group ions is even more shifted away from the Earth and its configuration differ significantly from the Figs. 1–4.

From a comparison of Figs. 1–2 with Figs. 5–6 one can see that for ions of CNO group the solar-cyclic (11-year) variations are greater than for protons. For example, at $L \sim 3$–5 from

https://doi.org/10.5194/angeo-2019-152
Preprint. Discussion started: 7 November 2019

Annales Geophysicae Discussions

maximum to minimum of solar activity fluxes of protons with $E > 1$ MeV practically do not changed, but the fluxes of the CNO group ions are increase by one order of magnitude and more. From a comparison of Figs. 3–4 with Figs. 5–6 it is seen also that the fluxes of CNO group ions varies by several times greater than the fluxes of helium ions.

This is mean that for ions of the CNO group the ionization losses at L = 3–5 are much larger than for ions with $Z \leq 2$ and these losses have a significant effect even on the power-law segment of the spectra of the CNO ions (in the part which is seen on Figs. 5–6). Therefore, the lower boundary of the power-law tail of these ions spectra is not monitored on the data given in Figs. 5 and 6. The red line on these figures is rather arbitrary: it corresponds to adiabatic laws that are not performed here, but this line let us to trace these deviations. As can be seen from fig. 5–6, ionization losses for ions of the CNO group are especially large at the maximum of solar activity (Fig. 6): in these times the slope of iso-lines on $L > 3$ is significantly less than the slope of the red line.

At the same time, at $L > 4$ in Fig. 5 and at $L > 3$ in Fig. 6 the iso-lines of fluxes pass almost parallel to each other and at approximately equal distances from each other; the average value of γ corresponding to them is ~ 6. Thus, for sufficiently large values of E and L, the CNO group ions spectra in the ERB have a power-law form, but these spectra are softer in comparison with the spectra of protons.

The red line corresponds here to the dependences $E_b/M_i \approx 43.4 \times L^{-3}$ MeV/n (on Fig. 5) and $E_b/M_i \sim 12.4 \times L^{-3}$ MeV/n (on Fig. 6), which are taken from (Kovtyukh, 2001) where this boundary was more clearly defined also for the ions of the CNO group. If one take into account that for the CNO group ions with $E > 0.1$ MeV/n at $L \sim$ 3–5 the average charge Q_i is +4 (see, e.g., Spjeldvik and Fritz, 1978), then for this boundary one can get: $\mu_b \sim 1.4 \times Q_i$ keV/n×nT^{-1} at the maximum of solar activity and $\mu_b \sim 1.4 \times M_i$ keV/n×nT^{-1} at the minima of solar activity (for the dipole magnetic field region).

3 Discussion

Let us consider the conclusions following from the results obtained here for solar-cyclic variations in the fluxes of ERB ions. Solar-cyclic (11-year) variations of proton fluxes with $E > 1$ MeV in the inner region of the ERB considered in many works (see, e.g., Pizzella et al., 1962; Hess, 1962; Blanchard and Hess, 1964; Filz, 1967; Nakano and Heckman, 1968; Vernov, 1969; Dragt, 1971; Huston et al., 1996; Vacaresse et al., 1999; Kuznetsov et al., 2010; Qin et al., 2014). These variations achieve one order of magnitude at L = 1.14 and reduce rapidly with increasing L (see, e.g., Vacaresse et al., 1999).

In these works, such variations of the proton fluxes of the inner belt are connected to the solar-cyclic variations of the energy loss rates of protons in this region. However, solar-cyclic variations of fluxes of ions with $Z \geq 2$ were not considered in these works.

In quiet periods, only the mechanism of ionization losses is significant for the ERB protons trapped on small L shells (see, e.g., Schulz and Lanzerotti, 1974). Energy loss rates and lifetimes of the ERB protons are determined in this mechanism by the density of atmospheric atoms and ionospheric plasma (N) in a geomagnetic trap. This density is depend on the intensity of the ultraviolet radiation of the Sun.

With decreasing solar activity (with a transition from maximum to minimum of the solar cycle), the densities of atmospheric atoms and ionospheric plasma in a geomagnetic trap are decreased. If the proton supply rates to the inner belt under the action of the CRAND mechanism remain unchanged or the effect of these changes is weaker than the effect connected with changes of loss rates of the protons, the stationary proton fluxes will increased with the solar activity decreasing.

The lifetimes of protons increase with L, and it lead to decreasing in the amplitude of the solar-cyclic variations of a proton fluxes. The proton lifetime on a given L shell depends on their energy

https://doi.org/10.5194/angeo-2019-152
Preprint. Discussion started: 7 November 2019

Annales Geophysicae Discussions

and is less than 11 years at $L < L^*(E)$. For example, for protons with $E \sim 10$ MeV the value L^* is ~ 2.5 (see, e.g., Kovtyukh, 2016a). Figs. 1 and 2 show that for protons the solar-cyclic variations of fluxes are small and localized at $L < 2.5$ (mainly at $L < 1.4$).

In contrast to protons, Figs. 3–6 show significant solar-cyclic variations of fluxes of helium ions and CNO group ions at $L \sim 2$–5. These variations one can explain by the same mechanism, which suggested for proton fluxes at $L < 2.5$.

For ions with $Z \geq 2$ in the ERB ionization losses are more significant than for protons. With this fact one can connect the absence of ions with $Z \geq 2$ at $L < 2$ (or very low values of these fluxes) during quiet geomagnetic conditions. More short lifetimes of these ions compare to protons are manifested also in the slope of the experimental curves in Fig. 4 and 6 (this was noted in sections 2.2 and 2.3, respectively). Consequently, for ions with $Z \geq 2$ the regions in which the solar-cyclic variations can manifested should be located on higher L shells (at the same energies as for protons).

The lifetimes of ions of the energies considered here are $\tau \propto M_i^{-1/2} Q_i^{-2} N^{-1} E^{3/2}$ (Schulz and Lanzerotti, 1974). In a first approximation, for $N \propto L^{-4}$, we obtain the value $L_i^* \sim (M_i^{1/2} Q_i^2)^{1./4} L^*$, where L^* corresponds to protons of the same energy as other ions. For helium ions ($M_i = 4$, $Q_i = 2$) with $E \sim 10$ MeV, we obtain $L_i^* \sim 4.2$. For ions of CNO group ($M_i = 14$, $Q_i = 4$) with $E \sim 10$ MeV we obtain $L_i^* \sim 6.9$. These is very rough estimates, but they correspond to results presented in Figs. 3–6.

These estimates are based on the following assumption: during variations in solar activity, the rates of ion supply on $L < L_i^*$ remain unchanged (or these changes are weaker than the effect of changes of the rate of ion losses). This assumption is real for protons with $E > 10$–20 MeV at $L < 2.2$: the fluxes of these protons forming mainly under the action of the CRAND mechanism. However, at $L > 2.2$ the stationary ion fluxes of the ERB forming mainly under the action of radial diffusion (see, e.g., Schulz and Lanzerotti, 1974; Kovtyukh, 2016b, 2018). Therefore, the solar-cyclic variations of fluxes for ions with $Z \geq 2$ one can explain only under the assumption that the effect connected with an increasing in the ionization losses of such ions significantly exceeds the effect connected with the possible enhance of radial diffusion of ions on the growth phase of solar activity.

In the experimental results presented here for the ERB ions, the region of the power-law tail of the ion spectra is distinguished. For many experiments, especially for heavy ions, the values of the parameter of a power-law tail spectra are determined much more accurately by the dependences $J(L)$ of the ion fluxes (in the logarithmic scale) for different pairs of energy channels (see Kovtyukh, 2001). For example, the range L in which these dependences for two energy channels are parallel to each other is corresponded to the power-law tail of the spectra. On smaller L these fluxes begin to converge and radial dependences of the fluxes intersect with each other which is corresponded to the maximum in the spectra. Consider here the physical mechanisms leading to the formation of power-law distributions of ions of the ERB.

The main source of ions in the outer regions of the ERB is the solar wind, and the high-energy part of these spectra have an exponential shape usually (see, e.g., Ipavich et al., 1981a, 1981b). Immediately before being captured into the magnetosphere, these ions pass through a highly turbulized regions, but the high-energy part of their spectra usually retains an exponential shape. Therefore, the question arises: what physical mechanism converts the form of ion spectra from exponential to power-law?

Evidently, the power-law tail of the ERB ions spectra must be generate-in the outer regions of the magnetosphere. The most likely region for this is the plasma sheet (PS) of the magnetospheric tail, which is adjacent to the geomagnetic trap. High-energy part of the ion spectra in the PS, at $R \sim 20$–40 R_E, have power-law shape and the exponents of these spectra is close to the corresponding parameters of the spectra of ions in the ERB. On the data of the satellites IMP-7 and IMP-8: Interplanetary Monitoring Platform 7 and 8 (Sarris et al., 1981; Lui et al., 1981) and also satellite ISEE-1 (Christon et al., 1991), the shape of the ion spectra of the PS usually do not changed during

https://doi.org/10.5194/angeo-2019-152
Preprint. Discussion started: 7 November 2019

substorms; they produce only parallel shifts of the spectra along logarithmic axes E and J. These results point out that the time scales of formation processes of these ion spectra in the PS are far exceeds the times of substorms.

Parameters of the power-law tail of the ion spectra of the outer belt (γ and μ_b) reflect, apparently, the most fundamental features of the mechanisms of acceleration of ions in the tail of the magnetosphere. One can try to connect the values of these parameters with the most general representations about the mechanisms and character of ion acceleration in the PS of the magnetospheric tail.

Most likely, this part of the ion energy spectra formed in the PS by stochastic mechanisms of the ion acceleration. This hypothesis supported by many experimental results. Statistical character of these mechanisms reveal itself, in particular, in the fact that the ratios of fluxes (and partial densities) of ions with different Z can be differ greatly at low and high energies. During wander in the phase space, ions gradually forget their origin and, therefore, the high-energy tails of the ion spectra do not contain unambiguous information on the partial densities of different components of ions in the source (see, e.g., Kovtyukh, 2001).

The high-energy part of the ion spectra of the PS can be generated by the mechanisms of acceleration of particles on magnetic irregularities moving relative to each other (Fermi mechanism). The fractal structures of the PS reveal itself on scales from ~ 0.4 to ~ 8 thousands kilometers, for example, in the data of the satellite Geotail (Milovanov et al., 1996). If mass of the ions are small compare to masses of the magnetic irregularities in the PS, the average values of the index γ of the power-law tail of the spectra should not depend on mass and charge of these ions.

Under equilibrium conditions, this parameter is determined by the average part of energetic ions in the total energy density of particles and magnetic irregularities ($\overline{\beta}$). From the theory which was developed by Ginzburg and Syrovatskii (1964), it is follows: $\gamma - 1 \approx (1 - \overline{\beta})^{-1}$. With increasing $\overline{\beta}$ in the interval $0 < \overline{\beta} < 1$, the value γ is increase monotonically and $\gamma \rightarrow \infty$ for $\overline{\beta} \rightarrow 1$. For real average values $\overline{\beta}$ in the central PS, we get $\gamma \sim 3.5$–7.0 ($\gamma \sim 4.3$ at $\overline{\beta} \sim 0.7$).

Spectra with power-law tail and quasi-exponential segment at lower energies can be generated when the value $\Delta B / \overline{B}$ for magnetic irregularities is proportional to their size δr and the spectral density of irregularities is decrease rapidly with increasing δr for $\delta r < r_s$, but for $\delta r > r_s$ it remains almost unchanged. Apparently, the spectra of magnetic irregularities in PS with thickness r_s have just such form. Then the lower boundary μ_b of the power-law tail is corresponded to the condition $r_s/\rho_i \sim 10$ (ρ_i is the gyroradius of ions), i.e. $\mu_b \sim 0.02(Q_i^2/M_i)B_s r_s^2$ keV nT^{-1}, where B_s is the average magnetic field induction in the PS (in nT) and r_s is normalized to the Earth's radius. Believing that $B_s \sim 30$ nT and $r_s \sim 1.3$ R$_E$ it can be obtained: $\mu_b \sim 1.0$ (Q_i^2/M_i) keV nT^{-1}.

The energy spectra of ions in the radiation belts of such planets as Jupiter and Saturn have the form analogous to the form of ion spectra in the ERB (see, e.g., Krimigis et al., 1981; Cheng et al., 1985). As that in the ERB, these spectra have a long power-law tail, which is formed, apparently, by mechanisms of stochastic acceleration of ions as a result of interactions of these ions with the current layer of the magnetospheric tail.

5 Conclusions

There are analyzed the experimental results for the stationary fluxes of the main ion components of the ERB (protons, helium ions and ions of the CNO group) in the near equatorially plane. It is found that in the outer belt these fluxes line up in the certain regular patterns in the space $\{E, L\}$. The degree of such similarity is increase with increasing E and L. The similarity of the spatial-energy distributions for various ionic components of the ERB is based on the main sources and on the universality mechanisms of transfer, acceleration and losses of ERB ions in the outer belt (radial diffusion while conserving μ and K of ions, betatron acceleration and ionization losses).

https://doi.org/10.5194/angeo-2019-152
Preprint. Discussion started: 7 November 2019

Solar-cyclic (11-year) variations of the spatial-energy distributions of the ERB ion fluxes are investigated. It is find that the ERB ions fluxes are weaken with increasing the solar activity and this effect increases with increasing an atomic number Z of the ions. Such a dependence of the amplitude of flux changes on Z is typical also for faster variations in the fluxes of the ERB ions, during geomagnetic storms and other disturbances of the Earth's magnetosphere, what is underlined in the review Kovtyukh (2018).

The figures presented here make it possible to determine in which regions of the space $\{E, L\}$ near the equatorial plane the ionization losses of ions during their radial diffusion can be neglect and where this cannot be done. These results indicate also that with variations in the level of solar activity the coefficient D_{LL} of the radial diffusion of the ERB ions change much less than the ionization losses rates of ions with $Z \geq 2$.

In addition, the figures given here reveal the localization of "white spots", especially extensive for ions with $Z \geq 2$ and $E > 1$ MeV/n at $L < 3$. The larger Z and energy of ions and the smaller L the greater the uncertainty in the values of the ERB fluxes. These gaps must be filled by the results of the future experiments on the satellites. Now the extensive gaps in the experimental data for fluxes of ions with $Z \geq 2$ do not allow create the sufficiently complete and reliable empirical models of the ERB for these ions.

Acknowledgements.

Financial support. This work was supported by Russian Foundation for Basic Research RFFI grant No. 17-29-01022.

References

Alfvén, H., and Fälthammar, C.-G.: Cosmical Electrodynamics, Fundamental Principles, Clarendon Press, Oxford, 1963.

Albert, J. M., Ginet, G. P., and Gussenhoven, M. S.: CRRES observations of radiation belt protons, 1, Data overview and steady state radial diffusion, J. Geophys. Res., **103**(A5), 9261–9273. https://doi.org/10.1029/97JA02869, 1998.

Blake, J. B., and Fennell, J. F.: Heavy ion measurements in the synchronous altitude region, Planet. Space Sci., **29**(11), 1205–1213, https://doi.org/10.1016/0032.0633(81)90125-2, 1981.

Blake, J. B., Fennell, J. F., Schulz, M., and Paulikas, G. A.: Geomagnetically trapped alpha particles, 2, The inner zone, J. Geophys. Res., **78**(25), 5498–5506, https://doi.org/10.1029/JA078i025p05498, 1973.

Blanchard, R. C., and Hess, W. N.: Solar cycle changes in inner-zone protons, J. Geophys. Res., **69**(19), 3927–3938, https://doi.org/10.1029/JZ069i019p03927, 1964.

Chenette, D. L., Blake, J. B., and Fennell, J. F.: The charge state composition of 0.4–MeV helium ions in the Earth's outer radiation belts during quiet times, J. Geophys. Res., **89**(A9), 7551–7555, https://doi.org/10.1029/JA089iA09p07551, 1984.

Cheng, A. F., Krimigis, S. M., and Armstrong, T. P.: Near equality of ion phase space densities at Earth, Jupiter, and Saturn, J. Geophys. Res., **90**(A9), 526–530, http://doi.org/10.1029/JA090iA01p00526, 1985.

Christon, S. P., Williams, D. J., Mitchell, D. G., Huang, C. Y., and Frank, L. A.: Spectral characteristics of plasma sheet ion and electron populations during disturbed geomagnetic conditions, J. Geophys. Res., **96**(A1), 1–22, https://doi.org/10.1029/90JA01633, 1991.

Croley, D. R., Jr., Schulz, M., and Blake, J. B.: Radial diffusion of inner-zone protons: Observations and variational analysis, J. Geophys. Res., **81**(4), 585–594, https://doi.org/10.1029/JA081i004p00585, 1976.

Dragt, A. J.: Solar cycle modulation of the radiation belt proton flux, J. Geophys. Res., **76**(10), 2313–2344, https://doi.org/10.1029/JA076i010p02313, 1971.

Fennell, J. F., and Blake, J. B.: Geomagnetically trapped α-particles, Magnetospheric Particles and Fields, edited by: McCormac, B. M., D. Reidel, Dordrecht, Holland, 149–156, 1976.
Filz, R. C.: Comparison of the low-altitude inner-zone 55–MeV trapped proton fluxes measured in 1965 and 1961–1962, J. Geophys. Res., **72**(3), 959–963, https://doi.org/10.1029/JZ072i003p00959, 1967.
Freden, S. C., Blake, J. B., and Paulikas, G. A.: Spatial variation of the inner zone trapped proton spectrum, J. Geophys. Res., **70**(13), 3113–3116, https://doi.org/10.1029/JZ070i013p03113, 1965.
Fritz, T. A., and Spjeldvik, W. N.: Observations of energetic radiation belt helium ions at the geomagnetic equator during quiet conditions, J. Geophys. Res., **83**(A6), 2579–2583, https://doi.org/10.1029/JA083iA06p02579, 1978.
Fritz, T. A., and Spjeldvik, W. N.: Simultaneous quiet time observations of energetic radiation belt protons and helium ions: The equatorial α/p ratio near 1 MeV, J. Geophys. Res., **84**(A6), 2608–2618, https://doi.org/10.1029/JA084iA06p02608, 1979.
Fritz, T. A., and Spjeldvik, W. N.: Steady-state observations of geomagnetically trapped energetic heavy ions and their implications for theory, Planet. Space Sci., **29**(11), 1169–1193, https://doi.org/10.1016/0032-0633(81)90123-9, 1981.
Ginzburg, V. L., and Syrovatskii, S. I.: The Origin of Cosmic Rays, Pergamon Press, Oxford, 1964.
Ginet, G. P., O'Brien, T. P., Huston, S. L., Johnston, W. R., Guild, T. B., Friedel, R., Lindstrom, C. D., Roth, C. J., Whelan, P., Quinn, R. A., Madden, D., Morley, S., and Su, Yi-J.: AE9, AP9 and SPM: New models for specifying the trapped energetic particle and space plasma environment, Space Sci. Rev., **179**(1–4), 579–615, https://doi.org/10.1007/s11214-013-9964-y, 2013.
Goka, T., Matsumoto, H., and Takagi, S.: Empirical model based on the measurements of the Japanese spacecrafts, Radiation Measurements, **30**(5), 617–624, https://doi.org/10.1016/S1350-4487(99)00237-1, 1999.
Hess, W. N.: Discussion of paper by Pizzella, McIlwain, and Van Allen, 'Time variations of intensity in the Earth's inner radiation zone, October 1959 through December 1960', J. Geophys. Res., **67**(12), 4886–4887, https://doi.org/10.1029/JZ0670i012p04886, 1962.
Hovestadt, D., Häusler, B., and Scholer, M.: Observation of energetic particles at very low altitudes near the geomagnetic equator, Phys. Rev. Lett., **28**(20), 1340–1343, https://doi.org/10.1103/PhysRevLett.28.1340, 1972.
Hovestadt, D., Gloeckler, G., Fan, C. Y., Fisk, L. A., Ipavich, F.M., Klecker, B., O'Gallagher, J. J., and Scholer, M.: Evidence for solar wind origin of energetic heavy ions in the Earth's radiation belt, Geophys. Res. Lett., **5**(12), 1055–1057, https://doi.org/10.1029/GL005i012p01055, 1978.
Hovestadt, D., Klecker, B., Mitchell, E., Fennell, J. F., Gloeckler, G., and Fan, C. Y.: Spatial distribution of $Z \geq 2$ ions in the outer radiation belt during quiet conditions, Adv. Space Res., **1**(1), 305–308, https://doi.org/10.1016/0273-1177(81)90125-3, 1981.
Huston, S., Kuck, G., and Pfitzer, K.: Low-altitude trapped radiation model using TIROS/NOAA data, Radiation Belts: Models and Standards, edited by: Lemaire, J. F., Heynderickx, D., and Baker, D. N., AGU, Washington, D. C., 119–122, https://doi.org/10.1029/GM097/p0119, 1996.
Ilyin, B. D., Kuznetsov, S. N., Panasyuk, M. I., and Sosnovets, E.N.: Non-adiabatic effects and boundary of the trapped protons in the Earth's radiation belts, Bulletin of the Russian Academy of Sciences: Physics, **48**(11), 2200–2203, 1984.
Ipavich, F. M., Galvin, A. B., Gloeckler, G., Scholer, M., and Hovestadt D.: A statistical survey of ions observed upstream of the Earth's bow shock: Energy spectra, composition, and spatial variation, J. Geophys. Res., **86**(A6), 4337–4342, https://doi.org/10.1029/JA086iA06p4337, 1981a.

Ipavich, F. M., Scholer, M., and Gloeckler, G.: Temporal development of composition, spectra, and anisotropies during upstream particle events, J. Geophys. Res., **86**(A13), 11153–11160, https://doi.org/10.1029/JA086iA13p11153, 1981b.

Kovtyukh, A. S.: Geocorona of hot plasma, Cosmic Res., **39**(6), 527–558, https://doi:10.1023/A:1013074126604, 2001.

Kovtyukh, A. S.: Radial dependence of ionization losses of protons of the Earth's radiation belts, Ann. Geophys., **34**(1), 17–28, https://doi.org/10.5194/angeo-34-17-2016, 2016a.

Kovtyukh, A. S.: Deduction of the rates of radial diffusion of protons from the structure of the Earth's radiation belts, Ann. Geophys., 34(11), 1085–1098. https://doi:10.5194/angeo-34-1085-2016, 2016b.

Kovtyukh, A. S.: Ion Composition of the Earth's Radiation Belts in the Range from 100 keV to 100 MeV/nucleon: Fifty Years of Research, Space Sci. Rev., **214**(8), 124:1–124:30, https:/doi.org/10.1007/s11214-018-0560-z, 2018.

Krimigis, S. M.: Alpha particles trapped in the Earth's magnetic field, Particles and Fields in the Magnetosphere, edited by: McCormac, B. M., D. Reidel, Dordrecht, Holland, 364–379, 1970.

Krimigis, S. M., Carbary, J. F., Keath, E. P., Bostrom, C. O., Axford, W. I., Gloeckler, G., Lanzerotti, L. J., and Armstrong, T. P.: Characteristics of hot plasma in the Jovian magnetosphere: Results from the Voyager spacecraft, J. Geophys. Res., **86**(A10), 8227–8257. http://doi.org/10.1029/JA086iA10p08227, 1981.

Kuznetsov, N. V., Nikolaeva, N. I., and Panasyuk, M. I.: Variation of the trapped proton flux in the inner radiation belt of the Earth as a function of solar activity, Cosmic Res., **48**(1), 80–85, https://doi.org/10.1134/S0010952510010065, 2010.

Lui, A. T. Y., and Krimigis, S. M.: Several features of the earthward and tailward streaming of energetic protons (0.29–0.5 MeV) in the Earth's plasma sheet, J. Geophys. Res., **86**(A13), 11173–11188, https://doi.org/10.1029/JA086iA13p11173, 1981.

Lutsenko, V. N., and Nikolaeva, N. S.: Relative content and the range of alpha particles in the inner radiation belt of the Earth by measurements on satellite Prognoz-5, Cosmic Res., **16**(3), 459–462, 1978.

McIlwain, C. E.: Coordinate for mapping the distribution of magnetically trapped particles, J. Geophys. Res., **66**(11), 3681–3691, https://doi.org/10.1029/JZ066i011p03681, 1961.

Milovanov, A. V., Zelenyi, L. M., and Zimbardo, G.: Fractal structures and power low spectra in the distant Earth's magnetotail, J. Geophys. Res. Space Phys., **101**(A9), 19903–19910, https://doi.org/10.1029/96JA01562, 1996.

Nakano, G., and Heckman, H.: Evidence for solar-cycle changes in the inner-belt protons, Phys. Rev. Lett., **20**(15), 806–809, https://doi.org/10.1103/PhysRevLett.20.806, 1968.

Northrop, T. G.: The Adiabatic Motion of Charged Particles, Wiley-Interscience, NY, USA, 1963.

Panasyuk, M. I., and Sosnovets, E. N.: Differential energy spectrum of low-energy protons in the inner region of the radiation belt, Cosmic Res., **11**(3), 436–440, 1973.

Panasyuk, M. I., Reizman, S. Ya., Sosnovets, E. N., and Filatov, V. N.: Experimental results of protons and α-particles measurements with energy more 1 MeV/nucleon in the radiation belts, Cosmic Res., **15**(6), 887–894, 1977.

Pizzella, G., McIlwain, C. E., and Van Allen, J. A.: Time variations of intensity in the Earth's inner radiation zone, October 1959 through December 1960, J. Geophys. Res., **67**(4), 1235–1253, https://doi.org/10.1029/JZ0670i004p01235, 1962.

Pizzella, G., and Randall, B. A.: Differential energy spectrum of geomagnetically trapped protons with the Injun 5 satellite, J. Geophys. Res., **76**(10), 2306–2312, https://doi.org/10.1029/JA076i010p02306, 1971.

Qin, M., Zhang, X., Ni, B., Song, H., Zou, H., and Sun, Y.: Solar cycle variations of trapped proton flux in the inner radiation belt, J. Geophys. Res. Space Phys., **119**(12), 9658–9669, https://doi.org/10.1002/2014JA020300, 2014.

https://doi.org/10.5194/angeo-2019-152
Preprint. Discussion started: 7 November 2019

Annales Geophysicae Discussions

Sarris, E. T., Krimigis, S. M., Lui, A. T. Y., Ackerson, K. L., Frank, L. A., and Williams, D. J.: Relationship between energetic particles and plasmas in the distant plasma sheet, Geophys. Res. Lett., **8**(4), 349–352, https://doi.org/10.1029/GL008i004p0349, 1981.

Schulz, M., and Lanzerotti, L. J.: Particle Diffusion in the Radiation Belts, Springer, NY, USA, 1974.

Selesnick, R. S., Hudson, M. K., and Kress, B. T.: Injection and loss of inner radiation belt protons during solar proton events and magnetic storms, J. Geophys. Res. Space Phys., **115**(A8), A08211, https://doi.org/10.1029/2010JA015247, 2010.

Selesnick, R. S., Baker, D. N., Jaynes, A. N., Li, X., Kanekal, S. G., Hudson, M. K., and Kress, B. T.: Observations of the inner radiation belt: CRAND and trapped solar protons, J. Geophys. Res. Space Phys., **119**(8), 6541–6552, https://doi.org/10.1002/2014JA020188, 2014.

Selesnick, R. S., Baker, D. N., Kanekal, S. G., Hoxie, V. C., and Li, X.: Modeling the proton radiation belt with Van Allen Probes Relativistic Electron-Proton Telescope data, J. Geophys. Res. Space Phys., **123**(1), 685–697, https://doi.org/10.1002/2017JA024661, 2018.

Spjeldvik, W. N.: Expected charge states of energetic ions in the magnetosphere, Space Sci. Rev., **23**(3), 499–538, https://doi.org/10.1007/BF00172252, 1979.

Spjeldvik, W. N., and Fritz, T. A.: Quiet time observations of equatorially trapped megaelectronvolt radiation belt ions with nuclear charge $Z \geq 4$, J. Geophys. Res., **83**(A9), 4401–4405, https://doi.org/10.1029/JA083iA09p04401, 1978.

Spjeldvik, W. N., and Fritz, T. A.: Observations of energetic helium ions in the Earth's radiation belts during a sequence of geomagnetic storms, J. Geophys. Res., **86**(A4), 2317–2328, https://doi.org/10.1029/JA086iA04p02317, 1981.

Stevens, J. R., Martina, E. F., and White, R. S.: Proton energy distributions from 0.060 to 3.3 MeV at 6.6 Earth radii, J. Geophys. Res., **75**(28), 5373–5385, https://doi.org/10.1029/JA075i028p05373, 1970.

Vacaresse, A., Boscher, D., Bourdarie, S., Blanc, M., and Sauvaud, J. A.: Modeling the high-energy proton belt, J. Geophys. Res. Space Phys., **104**(A12), 28601–28613, https://doi.org/10.1029/1999JA900411, 1999.

Venkatesan, D., and Krimigis, S. M.: Observations of low-energy (0.3– to 1.8–MeV) differential spectrums of trapped protons, J. Geophys. Res., **76**(31), 7618–7631, https://doi.org/10.1029/JA076i031p07618, 1971.

Vernov, S. N.: The Earth's radiation belts. In G. Bozóki, E. Gombosi, A. Sebestyén, A. Somogyi (Eds.), Proc. 11th ICRC, Budapest, 85–162, 1969.

Westphalen, H., and Spjeldvik, W.N.: On the energy dependence of the radial diffusion coefficient and spectra of inner radiation belt particles: Analytic solution and comparison with numerical results, J. Geophys. Res., **87**(A10), 8321–8326, https://doi.org/10.1029/2000JA087iA10p08321, 1982.

Wilken, B., Baker, D. N., Higbie, P. R., Fritz, T. A., Olson, W. P., and Pfitzer, K. A.: Magnetospheric configuration and energetic particle effects associated with a SSC: A case study of the CDAW 6 event on March 22, 1979, J. Geophys. Res., **91**(A2), 1459–1473, https://doi.org/10.1029/JA091iA02p01459, 1986.

Williams, D. J.: Phase space variations of near equatorially mirroring ring current ions, J. Geophys. Res., **86**(A1), 189–194, https://doi.org/10.1029/JA086iA01p00189, 1981.

Williams, D. J., and Frank, L. A.: Intense low-energy ion populations at low equatorial altitude, J. Geophys. Res., **89**(A6), 3903–3911, https://doi.org/10.1029/JA089iA06p03903, 1984.

Annales Geophysicae Discussions

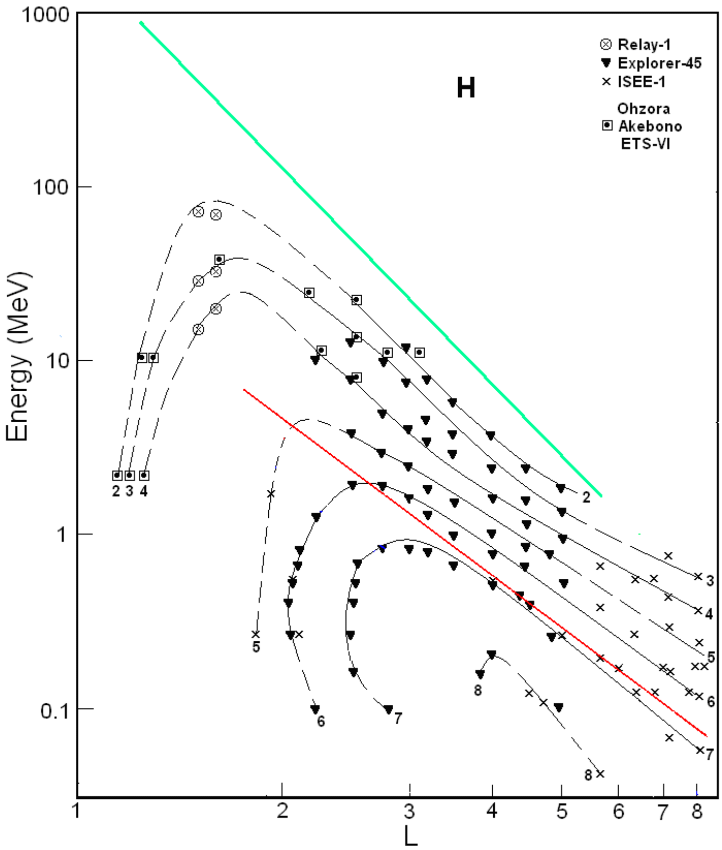

Figure 1. Proton fluxes in the ERB near minima of the solar activity. A numbers on the curves are equal the values of the decimal logarithms of J where J is given in (cm^2 s ster MeV)$^{-1}$; it is differential fluxes of protons with $\alpha_0 \approx 90^o$ (near the plane of the geomagnetic equator). Data of satellites are presented by different symbols. The red line corresponded to the lower boundary of the power-law tail of the proton spectra; green line corresponded to the maximum energy of protons trapped in the ERB (Ilyin et al., 1984).

https://doi.org/10.5194/angeo-2019-152
Preprint. Discussion started: 7 November 2019

Annales Geophysicae
Discussions
Open Access

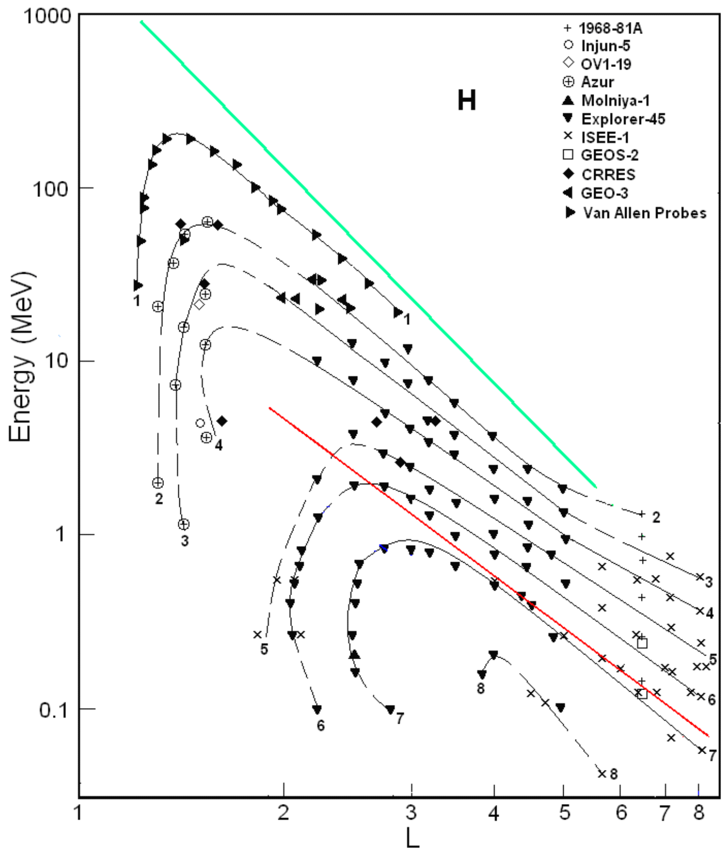

Figure 2. Proton fluxes in the ERB near maxima of the solar activity. A numbers on the curves are equal the values of the decimal logarithms of J where J is given in (cm^2 s ster MeV)$^{-1}$; it is differential fluxes of protons with $\alpha_0 \approx 90^o$ (near the plane of the geomagnetic equator). Data of satellites are presented by different symbols. The red line corresponded to the lower boundary of the power-law tail of the proton spectra; green line corresponded to the maximum energy of protons trapped in the ERB (Ilyin et al., 1984).

https://doi.org/10.5194/angeo-2019-152
Preprint. Discussion started: 7 November 2019

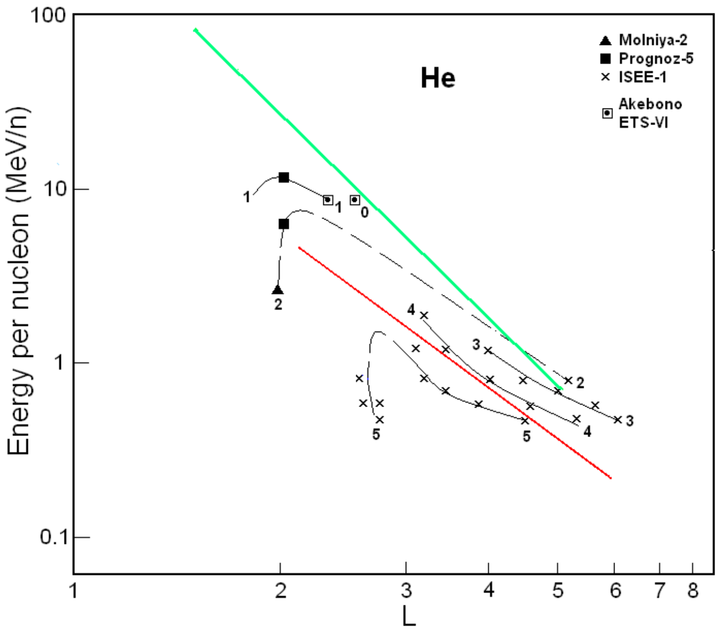

Figure 3. Helium ion fluxes in the ERB near minima of the solar activity. A numbers on the curves are equal the values of the decimal logarithms of J where J is given in (cm^2 s ster MeV/n)$^{-1}$; it is differential flux of protons with α_0 ≈ 90^o (near the plane of the geomagnetic equator). Data of satellites are presented by different symbols. The red line corresponded to the lower boundary of the power-law tail of the helium spectra; green line corresponded to the maximum energy of these ions trapped in the ERB (Ilyin et al., 1984).

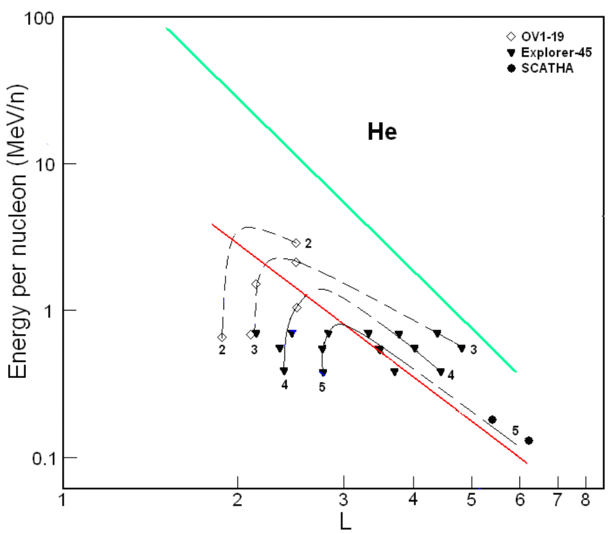

Figure 4. Helium ion fluxes in the ERB near maxima of the solar activity. A numbers on the curves are equal the value of the decimal logarithms of J where J is given in (cm^2 s ster MeV/n)$^{-1}$; it is differential flux of protons with α_0 ≈ 90^o (near the plane of the geomagnetic equator). Data of satellites are presented by different symbols. The red line corresponded to the lower boundary of the power-law tail of the helium spectra; green line corresponded to the maximum energy of these ions trapped in the ERB (Ilyin et al., 1984).

https://doi.org/10.5194/angeo-2019-152
Preprint. Discussion started: 7 November 2019

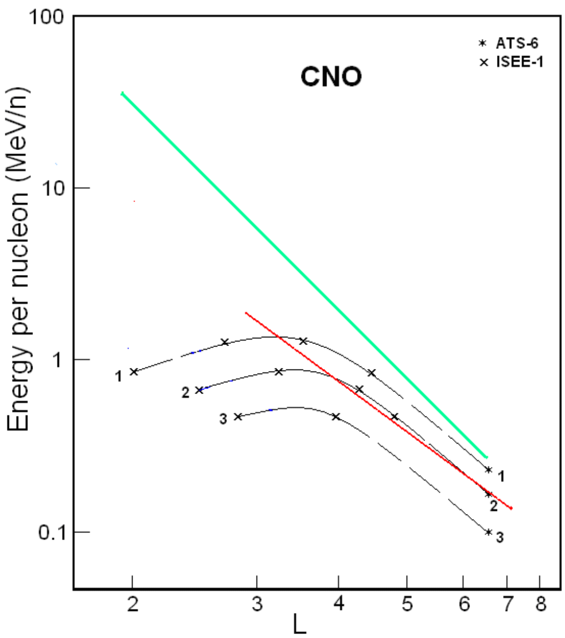

Figure 5. CNO ion fluxes in the ERB near minima of the solar activity. A numbers on the curves are equal the values of the decimal logarithms of *J* where *J* is given in (cm^2 s ster MeV/n)$^{-1}$; it is differential flux of protons with $\alpha_0 \approx 90^o$ (near the plane of the geomagnetic equator). Data of satellites are presented by different symbols. The red line corresponded to the lower boundary of the power-law tail of the CNO ion spectra; green line corresponded to the maximum energy of these ions trapped in the ERB (Ilyin et al., 1984).

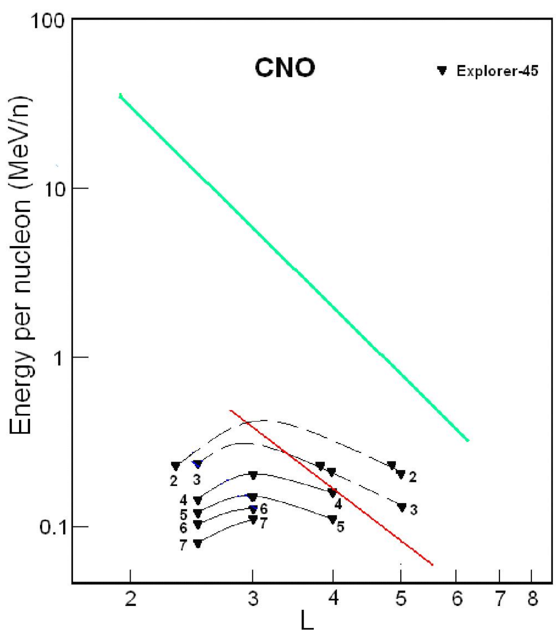

Figure 6. CNO ion fluxes in the ERB near the maximum of the solar activity. A numbers on the curves are equal the values of the decimal logarithms of *J* where *J* is given in (cm^2 s ster MeV/n)$^{-1}$; it is differential flux of protons with $\alpha_0 \approx 90^o$ (near the plane of the geomagnetic equator). Data of satellites are presented by different symbols. The red line corresponded to the lower boundary of the power-law tail of the CNO ion spectra; green line corresponded to the maximum energy of these ions trapped in the ERB (Ilyin et al., 1984).